INTEGRATION OF MULTI-SCALE MODELING OF COMPOSITES UNDER HIGH STRAIN RATE IMPACT WITH SURROGATE

By

SHU SHANG

A THESIS PRESENTED TO THE GRADUATE SCHOOL
OF THE UNIVERSITY OF FLORIDA IN PARTIAL FULFILLMENT
OF THE REQUIREMENTS FOR THE DEGREE OF
MASTER OF SCIENCE

UNIVERSITY OF FLORIDA

2013

To my parents

ACKNOWLEDGEMENTS

First, I would like to express my sincere gratitude to my advisor Professor Nam-Ho Kim for his patience and encouragement throughout my thesis. Without his guidance and persistent help this thesis would not have been possible.

I would like to thank my committee member, Professor Bhavani V. Sankar for his willingness to review my research and provide constructive comments to help me complete this thesis.

I thank Dr. Jinuk Kim since I've learned a lot from his work. I would also like to thank my lab colleagues and friends in Multidisciplinary Optimization Group: Jinsang Chung, Yongmin Chung and Susheel Kumar Gupta for their friendship and advices.

Most importantly, I would like to thank my parents for their love and continuous support throughout my life.

TABLE OF CONTENTS

Page

LIST OF TABLES

LIST OF FIGURES

Abstract of Thesis Presented to the Graduate School
of the University of Florida in Partial Fulfillment of the
Requirements for the Degree of Master of Science

INTEGRATION OF MULTI-SCALE MODELING OF COMPOSITES UNDER HIGH STRAIN RATE IMPACT WITH SURROGATE

By

Shu Shang

May 2013

Chair: Nam-Ho Kim
Major: Mechanical Engineering

The current trend of multi-scale modeling is based on massive parallel processing of micro-scale simulations. Macro-scale simulations require integrating the local response at various locations, i.e. integration points. At each integration point, micro-scale simulation is called to predict the material response. Since a huge number of integration points exist, it is often suggested to calculate the micro-scale simulation using massive parallel processing with a huge number of clusters. Although this architecture of simulation sounds attractive, a huge amount of computational resources are required. In addition, uncertainty quantification often requires numerous repetition of analysis which becomes easily impractical. In this research, instead of massive parallel processing, we propose to use surrogate modeling to bridge micro-scale simulation and structural scale simulation.

The material response under high strain rate impact has relatively been well studied for metallic materials. However, when it comes to composites materials, the mathematical model for failure becomes very complicated due to various failure modes as well as the statistical nature of manufacturing defects, which are much larger than that of metallic materials. The high strain rate impact of projectile on a composites panel

is highly localized and monotonic, thus there is no need to consider cyclic loading and unloading scenarios. Under high strain rate impact, the major failure mechanisms are fiber breakage, fiber debonding and pullout and delamination between adjacent plies. The first two mechanisms initiate at the fiber-matrix level and should be modeled in micro-scale, while delamination should be modeled in meso-scale and macro-scale. In micro-scale, an individual fiber and matrix is used to simulate fiber fracture and pullout, which contributes to the degradation of material properties in macro-scale. In macro-scale, high strain rate impact is simulated using nonlinear explicit finite element analysis using the degraded material properties from micro-scale simulation. Delamination is also included in macro-scale. This work does not cover macro-scale simulation. It will be done in further research.

At last, a high strain rate test from literature is used to validate the micro-scale simulation.

CHAPTER 1
INTRODUCTION

1.1 Multi-scale modeling of composite material

Composite materials are gaining increasing prominence in engineering applications. They allow to take advantage of different properties of component materials, of the layup configuration and of the interaction between the constituents to obtain a tailored behavior. Composite materials may present high stiffness and damping, improved strength and toughness, improved thermal conductivity and electrical permittivity, improved permeability, and unusual physical properties such as negative Poisson's ratio and negative stiffness inclusions [1].

For most of linear analyses of composite structures, instead of taking the individual constituent property and geometrical distribution into consideration, homogenized material properties are used. However, when higher accuracy is required, we need to refer directly to the microscopic scale. Then multi-scale modeling is needed to couple macroscopic and microscopic models to take advantage of the efficiency of macroscopic models and the accuracy of the microscopic models [2].

Most composite materials are multi-scale in nature, i.e. the scale of the constituents is of lower order than the scale of the structure. The length scales range from the fiber size whose dimension is measured in microns, to the individual plies in laminates whose thicknesses are measured in fractions of millimeters, to the laminates themselves whose sizes are measured in millimeters, e.g. 30-40 mm. The laminates then form parts of composite structures whose sizes are measured in meters. The physical phenomena observed at any of these length scales are linked to those on the neighboring length scales.

For fiber-reinforced composites, the overall hierarchy of multi-scale analysis is composed of micro-level (fibers and matrix), meso-level (plies) and macro-level (laminated composite). Since all damage and failure modes initiate in the micro-level, damage and failure criteria are applied to micro-level stresses and strains. At the constituent level, damage and failure modes are simplified and physics-based and there are three potential modes: fiber breakage, matrix cracking and interface debonding. At the macro-level, more complicated damage modes exist. For example, interlaminar delamination, matrix cracking in a cross-ply laminar and fiber splitting in a longitudinal layer are some of the potential damage modes. All of these are associated with matrix cracking. Each of these may require a different criterion and failure strength. However, when using micro-level damage criteria, all of these can be described using the same criterion associated with matrix cracking. As a result, damage and failure phenomena can be understood in unified and simplified concepts.

Currently there are two main approaches of multi-scale modeling:

I. Sequential multi-scale procedures. In this approach, the micro-to-macro homogenization process is made separately from the structural analysis. Material response is defined through a set of constitutive equations. Parameters in these equations are subsequently identified with microscopic or macroscopic results, either true experiments or virtual experiments.

II. Integrated multi-scale procedures. This approach deals with all the complexity of local microstructures during all analyses, without summarizing it in some overall constitutive framework. In such cases, at

each step of analysis, the actual response of each material point is calculated by calling for the micro-scale response, through the localization/homogenization process. To some extent, through an averaging scheme, the internal variables in the overall boundary value problem are those of the micro-scale unit cells used in this multi-scale numerical procedure.

Both approaches estimate the constitutive relationship at a macroscopic point by performing micro-scale finite element analysis on a representative volume element (RVE), assigned to that macro-scale point. Such work can be found in Smit [3], Feyel [4], Miehe et al. [5], Terada and Kikuchi [6]. Renard et al. [7] first introduced the idea of using directly a finite element discretization of the microstructure, linked to the macroscopic scale, using homogenization rules.

1.2 Motivation

Multi-scale modeling implements the largely intuitive notion that material response observed at a higher scale is determined by physical phenomena occurring at a lower scale [8]. A logical outcome of this thought is a hierarchy of scales. One of the major challenges is how to bridge the scales. Currently, typical multi-scale modeling techniques use parallel processing to couple the scales. However, this requires huge computational resources. Bridging three or more scales often necessitates unrealistic computing power even with the most versatile facilities available. Another situation is uncertainty quantification often requires numerous repetitions of response analyses, and it is easy to lose the feasibility of such huge computational resources.

1.3 Objective

The first objective of this work is to make a computer modeling technique for composite materials under high strain rate impact. The main contribution will be integrating micro-scale phenomena with macro-scale phenomena with the surrogate modeling technique to overcome the computational burden brought by massive parallel processing.

The second goal is to model the damage or failure phenomena under high strain rate loading which contribute to the degradation of material properties in the micro-scale simulation. Besides, strain rate effect on material properties need to be considered.

CHAPTER 2
UVE APPROACH FOR MODELING FIBER FRACTURE AND PULLOUT

2.1 Unite Volume Element

A variety of theories have been developed for micro-scale modeling of composite materials analytically, such as effective medium models of Eshelby [9], Hashin [10] and Mori and Tanaka [11]. And the traditional numerical method is representative volume element (RVE). A typical RVE of unidirectional fiber-reinforced composites is shown in figure 2-1. The analytical methods ignore the interaction among fibers by assuming that fiber is relatively small. This is not accurate since the nominal volume fraction of fiber is between 0.5 and 0.7, there exists a strong interaction between fibers. RVE assumes the periodic characteristics of fiber composites and applies the periodic boundary condition. However, when it comes to uncertainty quantification, RVE becomes inappropriate since periodicity in RVE works against fiber fracture and uncertainty in the layout of fibers. Uncertainty is caused by randomly distributed distance between fiber, but the periodicity enforces the distance in a certain pattern. In addition, the periodic boundary condition can often be inappropriate for composite plates. The dimensions in the membrane plane are large enough to be considered periodic, but the thickness direction of composite plates is relatively small, and the boundary effect becomes important in the response. In this research, instead of RVE, the unit volume element (UVE) is used. The major different between RVE and UVE is the boundary condition. UVE does not have periodic boundary condition in the thickness direction.

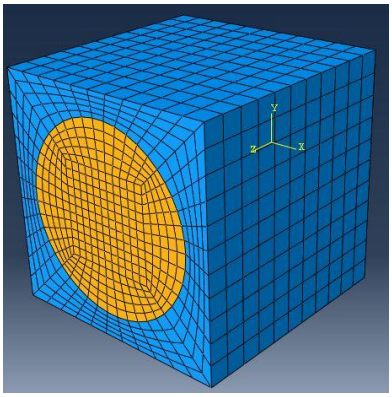

Figure 2-1. Structure of RVE of unidirectional fiber-reinforced composites.

2.1.1 Size of heterogeneous structure

The appropriate size of the heterogeneous structure should be decided first because the material behavior of the element placed at the most outer area would be different from the behavior of the one placed in the middle of the structure.

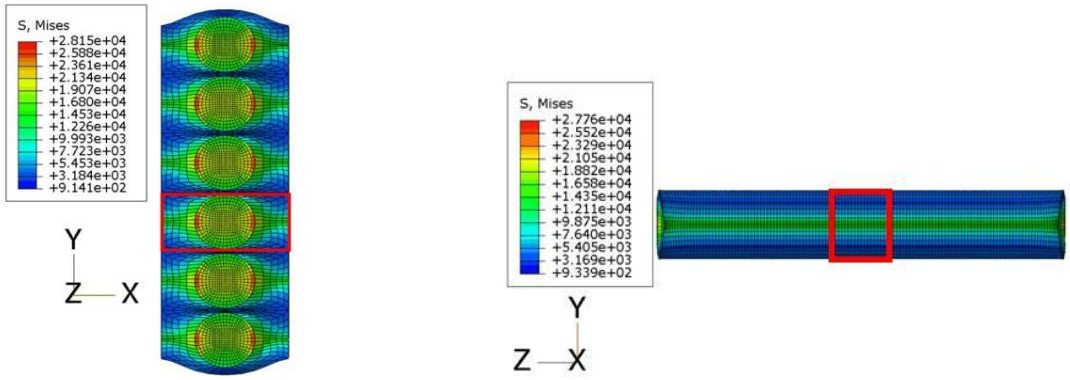

A B

Figure 2-2. Heterogeneous structure composed of UVE piled up. A) Y direction. B) Z direction.

Figure 2-2 shows the deformed shape of the structures composed of several fibers in y direction and z direction under x direction displacement loading respectively [12]. Jinuk Kim [12] found out that three UVEs in y direction and z direction should be enough for the size of the heterogeneous structure by comparing the effective stress in

UVEs at different position. The heterogeneous structure model in this research is shown in Figure 2-3. The mesh is composed of 29889 linear hexahedral elements of type C3D8 in Abaqus.

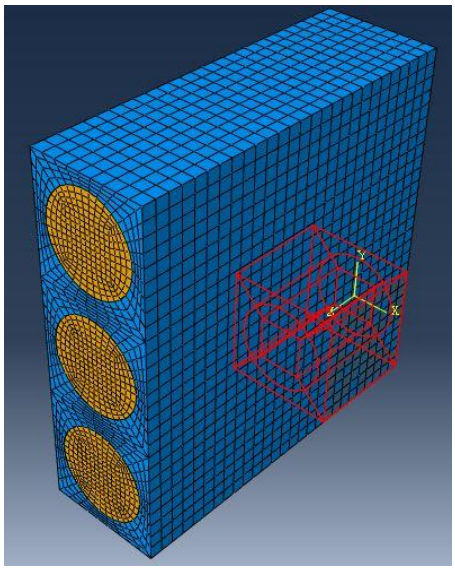

Figure 2-3. Heterogeneous structure model.

2.1.2 Boundary conditions

The dimension in x direction is large enough to be considered periodic. And periodic boundary conditions will be imposed on the two surfaces perpendicular to x axis. The periodic boundary condition constrains the boundary to keep the relative displacement constant according to the strain on that boundary. It can be expressed as follows:

$$u_i(x_0 + d) = u_i(x_0) + \bar{\varepsilon}_{ij} d_j \quad (1)$$

where $\bar{\varepsilon}_{ij}$ is the average strain component and d is the characteristic distance.

Besides the periodic boundary condition, other boundary conditions are needed to remove rigid body motion of the structure. Figure 2-4 shows the boundary conditions applied to the UVE.

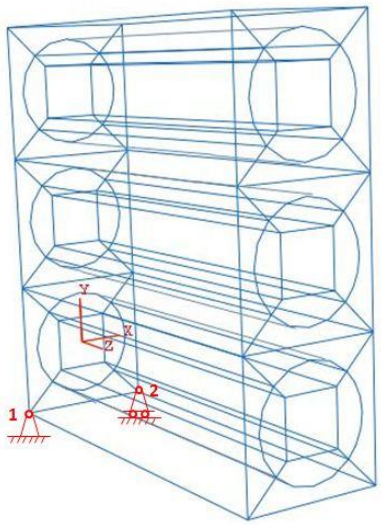

Figure 2-4. Boundary conditions applied to remove rigid body motion.

Point 1 is pinned. Translation motion of point 2 in z direction is constrained. And symmetric boundary condition is applied to the bottom surface.

2.1.3 Average stress values

The average scheme is used to calculate representative stress values of the UVE,

$$\bar{\sigma}_{ij} = \frac{1}{V}\int_V \sigma_{ij} dV \tag{2}$$

where σ_{ij} is the local stresses in the UVE or micro stresses.

As UVE itself is composed of small elements, the average can be achieved by integrating individual elements. In order to perform volume integral of each element, the Gaussian integration method is applied

$$\bar{\sigma}_{ij} = \frac{1}{V}\sum_{i=1}^{NE}\int_V \sigma_{ij} dV_i = \frac{1}{V}\sum_{i=1}^{NE}\sum_{k=1}^{8}\frac{(\sigma_{ij})_k}{8} V_e \tag{3}$$

where NE is the number of element, V_e is the volume of single element.

Since the material behavior of UVE placed at the most outer area would be different from the behavior of the one placed in the middle of the structure, average stress of inner part of the structure will be calculated, as shown in Figure 2-5.

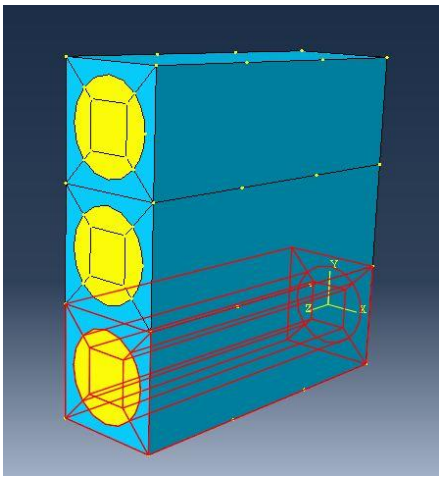

Figure 2-5. Inner part of heterogeneous structure.

2.2 Modeling of major damage modes

Under high strain rate loading, the major failure mechanisms are fiber breakage, fiber debonding and pullout and delamination. Figure 2-6 shows the major failure modes observed in actual experiments. From this figure, we can see that fiber breakage and debonding both initiate and can be observed in the micro scale and will be modeled in the UVE. However, delamination between plies, though associated with matrix cracking initiated from the micro scale, is observed in the meso scale and thus will not be modeled in the unit cell.

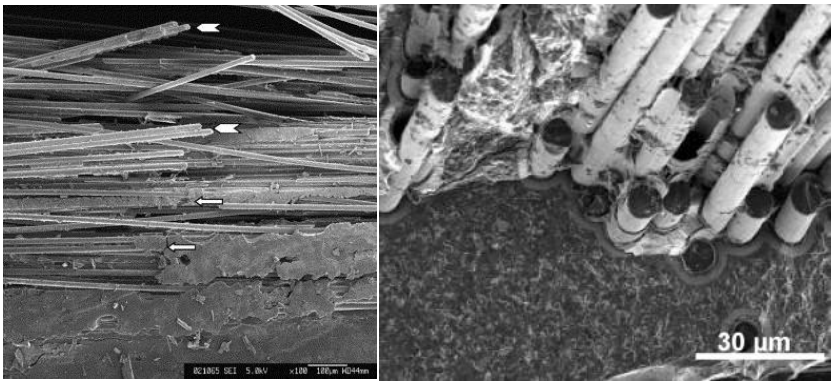

(a) (b)

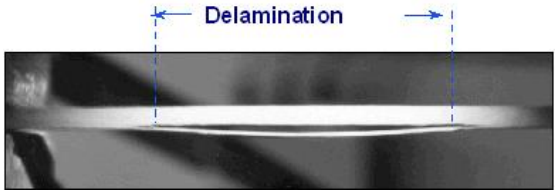

(c)

Figure 2-6. Major failure modes under high strain rate impact: (a) fiber breakage; (b) fiber debonding and pullout; (c) delamination.

2.2.1 Modeling of fiber fracture

Fiber carries most of the load and thus fiber fracture contributes most to the degradation of material properties. In this research, the crack in the fiber is modeled as enriched feature of finite elements. The extended finite element method (XFEM) uses the enriched feature and is an extension of general FEM allowing the discontinuities to exist in an element by enriching degrees of freedom with special displacement functions. This method is efficient especially when crack propagation is to be investigated since it does not require remeshing as fracture of fiber progresses.

Under high strain rate impact, fiber behaves as brittle material and fiber fracture occurs completely in an extremely short time period. Figure 2-7 shows the stress-strain

curve of a common carbon fiber T300 under different strain rates [19]. We can see that the curve is composed of elastic region and sudden fracture. And since the degradation due to fiber fracture is the focus, the propagation of the crack is not considered. Stationary crack can be defined using an enrichment command and assigning crack domain in Abaqus. When the elements are intersected by the defined stationary crack domain, the elastic strength of that element is regarded as zero, which can be regarded as discontinuous. Figure 2-8 shows the assignment of a stationary crack and the stress field near the crack front [12].

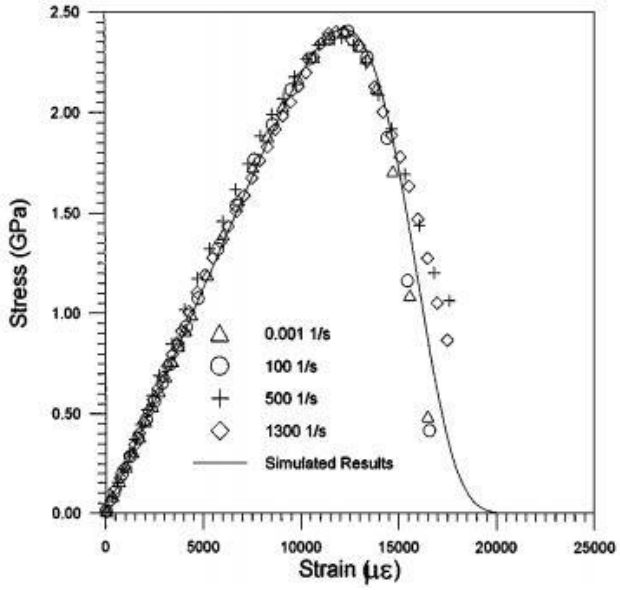

Figure 2-7. Stress-strain curve of T300 under different strain rates.

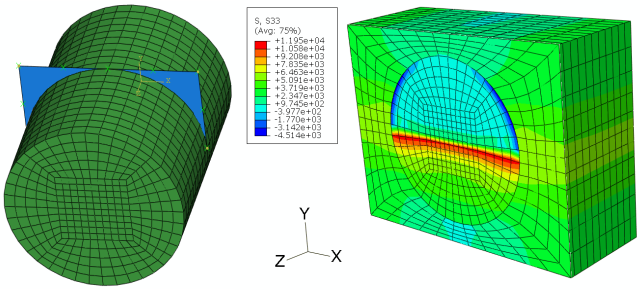

Figure 2-8. Transverse direction crack in fiber.

2.2.2 Modeling of fiber debonding and pullout

Interfacial property between fiber and matrix has a great influence on the performance of a composite. In addition, the interfacial property contributes to a lot of randomness in material behavior. The interface plays a significant role in stress transfer between fiber and matrix. In unidirectional composites, debonding occurs at the interface between fiber and matrix when the interface is weak. The interfacial debonding behavior of single-fiber composites has been studied in detail in [13, 14, 15].

Fiber debonding and pullout can be simulated using cohesive zone elements [16]. Cohesive zone elements do not represent any physical material, but describe the cohesive forces which occur when material elements are being pulled apart. Cohesive zone elements are placed between continuum (bulk) elements, as shown in Figure 2-9.

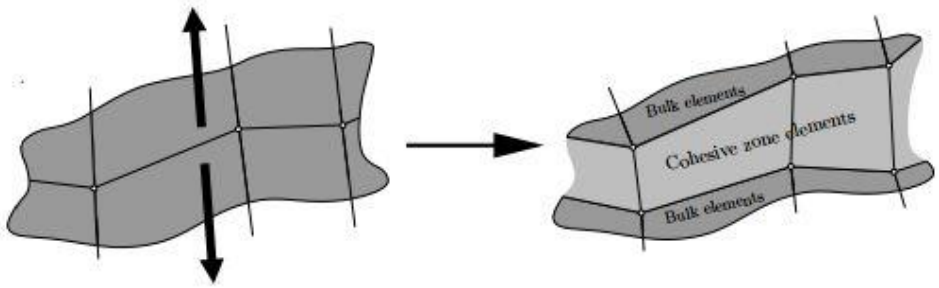

Figure 2-9. Application of cohesive zone elements along bulk elements boundaries.

When damage growth occurs, these cohesive zone elements open in order to simulate crack initiation or crack growth. The description of the failure behavior is defined by the traction-separation law, which describes the traction as a function of separations and determines the constitutive behavior of cohesive zone elements. There are various traction-separation laws but they all exhibit the same global behavior. The traction first increases with separation until a maximum point, and subsequently decreases to zero which implies complete separation. This holds for both the normal

and shear direction. A simple example of a traction-separation curve is shown in Figure 2-10.

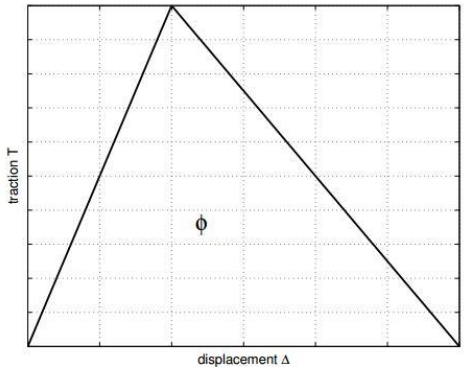

Figure 2-10. Example of traction-separation curve.

Since the crack path can only follow these elements, the direction of crack propagation strongly depends on the presence (or absence) of cohesive zone elements, implying the crack path is mesh dependent. Thus we can model fiber debonding and pullout by simply placing a layer of cohesive elements between fiber and matrix. Figure 2-11 shows the deformed shape of cohesive elements.

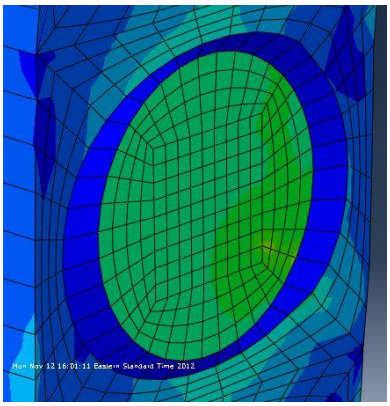

Figure 2-11. Deformed shape of cohesive zone elements.

2.3 Strain rate effect on material property

As mentioned earlier, this research focuses on a high strain rate impact phenomenon. Strain rate might have a big effect on the material response. High strain rates tend to favor the elastic properties of materials. Elasticity is associated with load-bearing performance as embodied in properties such as strength and stiffness. However, low strain rates favor the viscous or energy-damping aspects of material behavior. Viscous flow is associated with energy management, often referred to as impact resistance or toughness.

For composite materials, fibers are the main load-bearing elements and reliable information of the properties of fibers under high strain rate loading is important. Because of technical difficulties in tests, currently, it is difficult to obtain the dynamic properties of a single fiber directly. Chi et al. [17] proposed an approach for determining the static properties of single fiber by measuring those of fiber bundles. Xia et al. [18] extended the method to dynamic state and first successfully performed tensile impact tests on fiber bundles. Their testing strain rate was up to 1100/s. One of the most popular types is carbon fiber. Table 2-1 shows mechanical properties of two common carbon fibers, T300 and M40J, at different strain rates [19]. It can be observed that for these two kinds of carbon fibers the effect of strain rate on material property can be ignorable. However, for other kinds of fibers, the effect of strain rate might be very prominent. Figure 2-12 shows the relationship between strain rate and the ultimate strength of M40J, T300, E-glass and Kevlar49 fiber bundles [19]. It can be concluded that M40J and T300 are strain rate insensitive materials while E-glass and Kevlar49 are sensitive to strain rate.

Table 2-1. Mechanical properties of T300 and M40J at different strain rates.

	$\dot{\varepsilon}$ (s^{-1})	E (GPa)	$\lvert\Delta E/E\rvert$	ε_b (100%)	$\lvert\Delta\varepsilon_b/\varepsilon_b\rvert$	σ_b (GPa)	$\lvert\Delta\sigma_b/\sigma_b\rvert$
M40J	0.001	357.9	2.3%	1.26	4.1%	3.339	3.2%
	100	359.6	2.5%	1.28	2.2%	3.336	2.6%
	500	360.1	2.0%	1.29	2.3%	3.354	1.2%
	1300	359.1	2.1%	1.29	3.4%	3.347	2.6%
	Average value	359.2	---	1.28	---	3.344	---
T300	0.001	223.2	4.5%	1.35	4.1%	2.387	3.6%
	100	227.4	3.7%	1.32	4.0%	2.415	3.2%
	500	223.5	3.4%	1.34	3.6%	2.404	2.8%
	1300	225.6	4.1%	1.34	3.7%	2.418	3.4%
	Average value	224.9	---	1.34	---	2.406	---

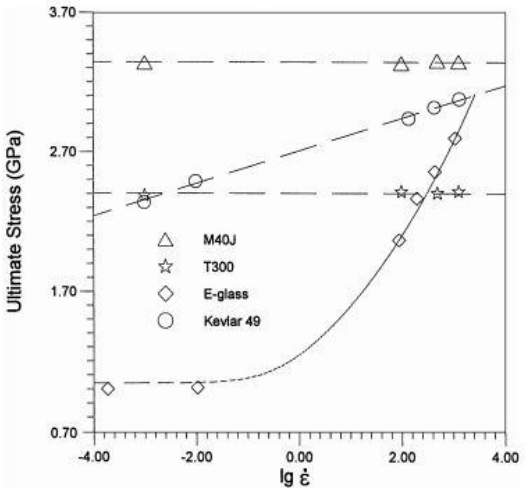

Figure 2-12. Effect of strain rate on ultimate strength of fiber bundles.

The matrix phase for fiber reinforced composites can be a metal, polymer or ceramic. Generally, the matrix works as binding materials that supports and protects fibers. And metals and polymers are usually used as a matrix because of ductility. However, under high strain rate impact, ductile materials tend to behave as a brittle material. Figure 2-13 shows experimental tensile stress-strain curves for PR520 resin,

which is commonly used as a matrix, at different strain rates [20]. This figure indicates that as strain rate increases, ductility tends to vanish.

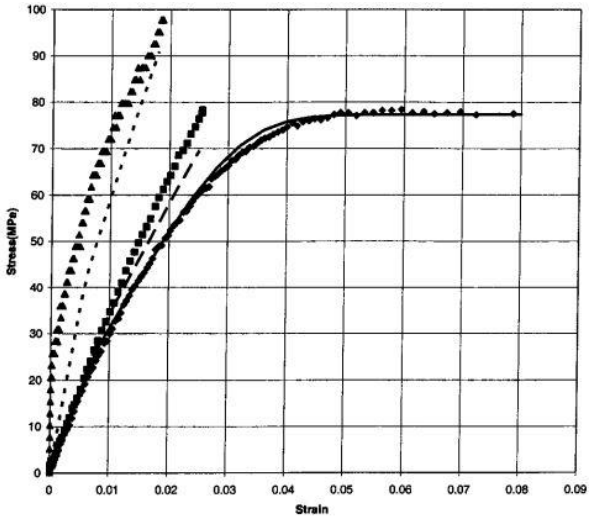

Figure 2-13. Experimental tensile stress-strain curves for PR520 resin at strain rates of 5x10-5/s (low rate), 1.4/s (medium rate) and 510/s (high rate).

For both fiber and matrix, linear elastic model will be used for simplicity. As mentioned in previous section, fracture of fiber will be modeled using extended finite element method. Damage and fracture of matrix is not the focus here since fiber is the main load-bearing element.

CHAPTER 3
SURROGATE MODELING OF COMPOSITES CONSTITUTIVE RESPONSE

3.1 Kriging surrogate

In this research, we propose to integrate micro-scale simulation with macro-scale phenomena with a surrogate modeling technique. As one of the most popular surrogates, kriging is used to estimate the behavior of the micro-structure. In addition, the surrogate can also be used to estimate uncertainty in micro-structure.

3.1.1 Modeling and prediction

Following [21], we adopt a model that treats the deterministic response y(x) as a realization of a random function (stochastic process) and a regression model,

$$\hat{y}(x) = \sum_{j=1}^{k} \beta_j f_j(x) + Z(x) \tag{4}$$

The random process Z(x) is assumed to have mean zero and covariance

$$V(w, x) = \sigma^2 R(\theta, w, x) \tag{5}$$

between Z(w) and Z(x), where σ^2 is the process variance and $R(\theta, w, x)$ is the correlation model with parameter θ.

The common functions $f_j(x)$ used in regression model are polynomial with orders 0, 1 and 2. And the most popular correlation function is Gaussian correlation function which takes the form

$$R(\theta, w, x) = \prod_{j=1}^{n} exp[-\theta_j (w_j - x_j)^2] \tag{6}$$

The optimal coefficients θ of the correlation function can be found by solving

$$min\ (detR)^{1/n} \sigma^2 \tag{7}$$

3.1.2 Design of experiments

Experimental design is important since it decides how to select the inputs at which to run the analysis in order to most efficiently reduce the statistical uncertainty of the prediction. Latin hypercube sampling (LHS) will be used here.

Latin hypercube sampling, due to McKay et al. [22], is a statistical method for generating random samples from a multidimensional distribution ensuring that all portion of the design space is represented. Consider the case where we wish to sample *m* points in the *n* dimensional space. The Latin hypercube sampling strategy can be explained as follows:

1. Divide the interval of each dimension into *m* non-overlapping intervals having equal probability (e.g. for uniform distribution, the intervals should have equal size).
2. Sample randomly from the distribution a point in each interval in each dimension.
3. Pair randomly (equal likely combinations) the point from each dimension.

3.2 Surrogate modeling

As mentioned earlier, we use Latin hypercube sampling strategy to generate different combinations of strain components at which to run the simulation in Abaqus and calculate the average stresses. In Abaqus, in order to apply random strain values, equation constraint is used in python script to control translational degrees of freedom of all the nodes on the boundary.

With strain values as input and stress values as output, we can construct a kriging surrogate for each stress component. This can be done using a Matlab kriging

toolbox DACE [23]. In Chapter 2, we have already mentioned that crack propagation in the fiber is not going to be investigated, only the degradation due to fiber fracture is the focus. We will have two UVE models with intact fiber and totally fractured fiber respectively, thus for each stress component two kriging surrogate will be constructed. Now, we need a criterion to determine when given certain strain values as input which UVE model should be called, i.e. we need a criterion to determine when fiber fracture happens. First we assume that axial stress, which leads to fiber fracture, is determined by axial strain only. To verify the accuracy of this assumption, we use LHS to generate samples of input, run the analysis, calculate the average stress and project all points on $\varepsilon_{33}/\sigma_{33}$ plane. Here, 3 stands for the axial direction. Figure 3-1 shows the data points and linear regression. However, it is clear that the error is not ignorable. The RMS error is 100.3, 10.93% of the average value of σ_{33}. Notice that when ε_{33} is zero, the value of the fitted linear function is about 250, which means that we cannot ignore the contribution of other strain components to axial stress.

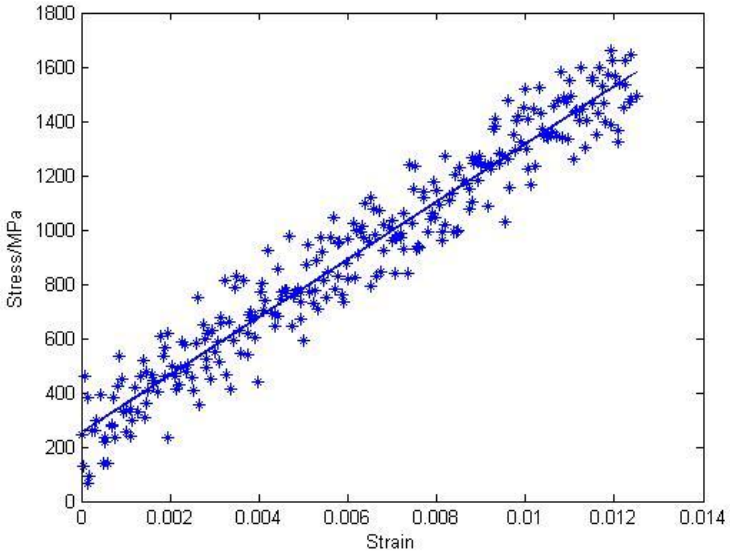

Figure 3-1. $\varepsilon_{33}/\sigma_{33}$ data points and linear regression.

Taking Poisson's effect into consideration, instead of using ε_{33} directly, we should use an equivalent $\bar{\varepsilon}_{33}$,

$$\bar{\varepsilon}_{33} = \nu_{13}\varepsilon_{11} + \nu_{23}\varepsilon_{22} + \varepsilon_{33} \tag{8}$$

where ν_{13} and ν_{23} are effective Poisson's ratios obtained from homogenization of elastic behaviors. Now project all points on $\bar{\varepsilon}_{33}/\sigma_{33}$ plane. Figure 3-2 shows the modified data points and linear regression.

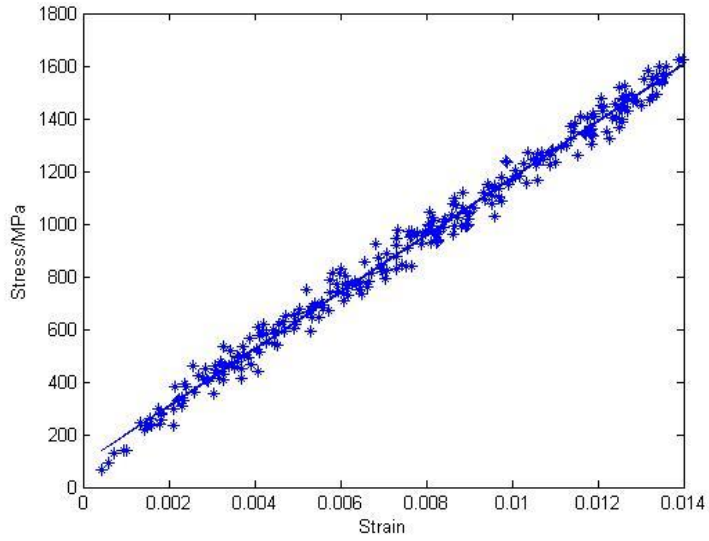

Figure 3-2. $\bar{\varepsilon}_{33}/\sigma_{33}$ data points and linear regression.

With $\bar{\varepsilon}_{33}$, the RMS error reduces to 40.857, 4.45% of the average value of σ_{33}. And when $\bar{\varepsilon}_{33} = 0$, the value of the linear function is about 91MPa. It is accurate enough to use the equivalent axial strain as the fiber fracture criterion. By comparing $\bar{\varepsilon}_{33}$ with a certain critical value, we can decide which UVE model should be called so that all the inputs can be divided into two groups and two kriging surrogates can be constructed for each stress component.

CHAPTER 4
MULTI-SCALE MODELING OF HIGH STRAIN RATE COMPOSITES RESPONSE

A composite panel is composed of many laminates with different fiber orientations. And a laminate is composed of many fibers through the thickness. A significant gap exists between the size of initiating fracture and the size of design interest, thus how to propagate information in micro scale to macro scale is a critical issue. As mentioned earlier, in this research, instead of massive parallel processing, we propose to use surrogate modeling to bridge micro-scale simulation and structural scale simulation to overcome the computational burden.

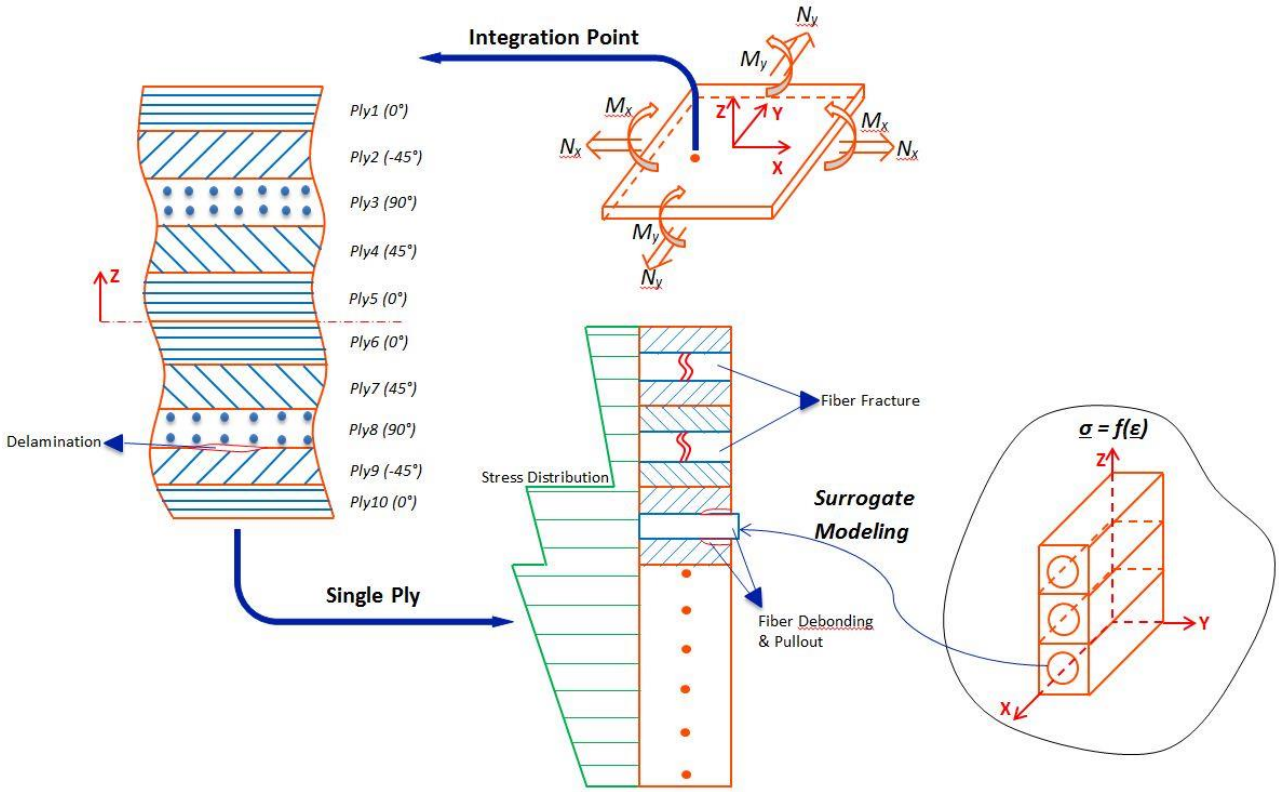

Figure 4-1. Illustration of multi-scale modeling.

The basic idea of multi-scale modeling is illustrated in Figure 4-1, in which a composite panel is decomposed into three levels: composite panel, ply, and fiber-matrix cell. In the composite panel level, the material behaves similar to anisotropic material. In

this scale, finite element analysis is often used to simulate the global response of composite panel, which requires calculating stresses at integration points of each element. It is possible that some fibers are broken and debonding may occur between a fiber and matrix. The macro-scale stress calculation should include all these effects. Therefore, the multi-scale modeling is performed at each Gauss point of the FE mesh of the overall structure.

In the ply level, different directions of ply stacking sequence are considered in calculating the distribution of stress along the thickness direction. In this report, 10 plies with lay-up configuration $[0/-45/90/45/0]_s$ are used. Strain calculated in the panel level is converted to strain at each ply. The strain at different locations of a ply is then sent to fiber-matrix cell level to calculate stress at that location. Since the fiber direction changes at different plies, coordinate transformation must be performed to convert strains and resulting stresses between the local and global coordinate system. Also notice that delamination between plies initiates in this scale. However, this failure mode is not covered since the focus of current work is micro-scale modeling and propagating information in the micro-scale to macro-scale using surrogate modeling technique.

In the fiber-matrix level, fiber and matrix phases are modeled separately. Two major failure modes, fiber fracture and fiber debonding, are considered. As described in chapter 2, fiber fracture is modeled using extended finite element method and fiber debonding is modeled by cohesive element which is governed by traction-separation law. The interfacial property between fiber and matrix is crucial here. However, it is difficult to obtain this property through experiments. Here, matrix property is assumed as upper bound of property of cohesive elements and traction-separation law is derived

from the matrix property. In this scale, with strain values sent from higher level, UVE approach is used to calculate effective stresses. Instead of massive parallel processing, kriging surrogate is constructed with strain inputs generated from LHS sampling and stress outputs calculated from UVE model analyzed in Abaqus. The multi-scale surrogate modeling technique proposed here can overcome the computational burden in typical multi-scale modeling technique and provide feasibility to uncertainty analysis based on large amount of repetition of response analysis in future research.

CHAPTER 5
NUMERICAL STUDY AND VALIDATION

Characterization of material property at high strain rates above 100 s^{-1} is difficult because of nonhomogeneous deformation in the specimen (stress wave effects have to be considered) and the inability to measure force and deformation directly. Kolsky [24] introduced the split Hopkinson bar which is the most widely used technique for a direct determination of material properties at strain rates between 200 and 10^4 s^{-1}.

In this chapter, experimental results from literature [25] will be used to validate the micro-scale model. In this paper, high strain rate tests (approximately 1000 s^{-1}) are conducted using a direct tension split Hopkinson bar apparatus. A schematic representation of the apparatus is shown in Figure 5-1. A tensile wave is generated in the input bar by release of a load initially stored in the section between the clamp and the end of the bar. The specimen is a rectangular $[\pm\theta]_s$ laminates made from Scotchply 1002, θ equals to 15°, 30°, 45°, 60° and 75° respectively. Dog-bone shape coupons were cut from the laminates, glued to two slotted cylinders, and subsequently cemented between the input and output bars. Figure 5-2 shows the dog-bone coupon and slotted cylinder holder.

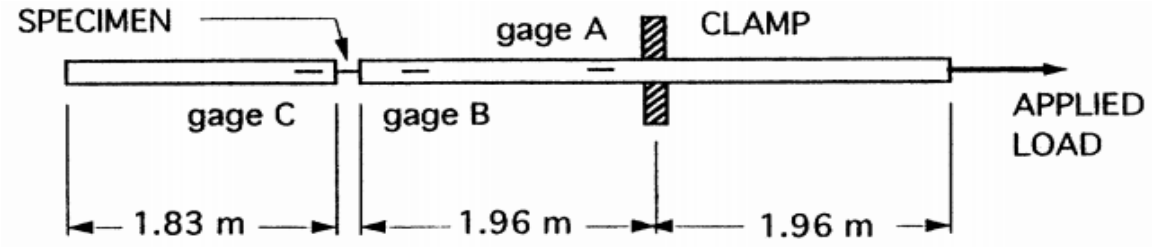

Figure 5-1. Schematic of direct tension Hopkinson bar apparatus.

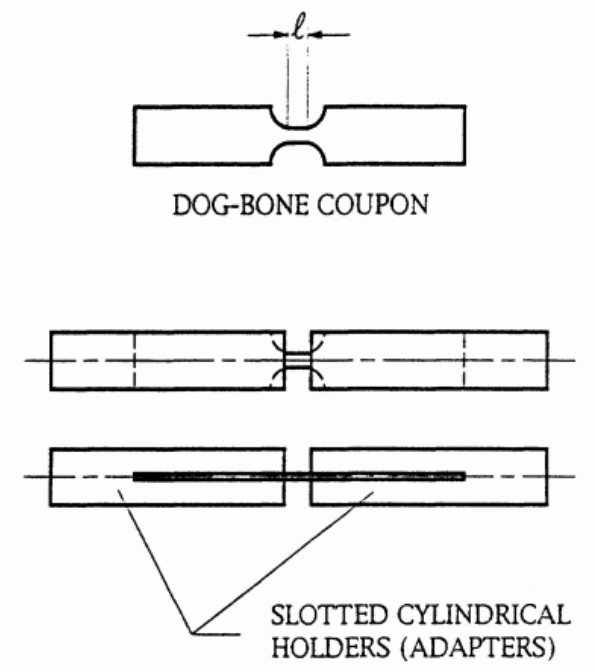

Figure 5-2. Schematic of dog-bone specimen and slotted cylindrical holder for dynamic tests.

The whole history of strain rate, strain and stress in the specimen during the test will not be simulated, instead only the maximum strain and stress obtained during the test will be used for validation. Table 5-1 shows a summary of experimental results. We can see that for specimen $[\pm 15^{\circ}]_s$ the maximum strain seems unrealistic. This is because in the split Hopkinson bar tests the strain is determined from the relative velocity of the holders' ends between which the specimen is mounted. It is assumed that the relative displacement of the holders' ends is entirely due to the deformation of the specimen. However, the specimen is actually connected to the holders by gluing the end tabs in the holders' slots. For specimen $[\pm 15^{\circ}]_s$, the load transmitted through the connection is much larger than other specimens and the maximum strain in this case is unrealistic, thus this data should be abandoned. The fiber used in Scotchply 1002 is E-glass fiber. Property of E-glass under high strain rate loading can be found in [26]. Table

5-2 shows mechanical properties of E-glass fiber bundles under different strain rates. However, the type and property of epoxy resin used in the specimen is unknown. The $[\pm 75^{\circ}]_s$ specimen data will be used for calibration because the stress in this specimen is smallest and the error in strain value is also smallest.

Table 5-1. Summary of experimental results.

Specimen Type	$\dot{\varepsilon}$ (s^{-1})	σ_{max} (MPa)	ε_{max}
$[\pm 15^{\circ}]_s$	1403	924	20.0%
$[\pm 30^{\circ}]_s$	1069	482	5.80%
$[\pm 45^{\circ}]_s$	996	207	5.30%
$[\pm 60^{\circ}]_s$	1310	131	2.60%
$[\pm 75^{\circ}]_s$	1024	79	0.60%

Table 5-2. Mechanical properties of E-glass fiber bundles under different strain rates.

$\dot{\varepsilon}$ (s^{-1})	90	300	800	1100	1300	1700
σ_b (GPa)	2.15	2.50	2.75	2.85	2.93	2.99
ε_b (%)	3.70	4.00	4.30	4.40	4.41	4.11
E (GPa)	69.397	74.832	76.736	77.30	78.00	84.40

Since only axial strain is known, applying maximum strain to the model to predict the maximum stress is no longer applicable. Instead, the specimen is under plane stress condition, stress values are known. Maximum stress should be used to predict the maximum strain, thus compliance matrix is be needed. We need to calculate

stiffness matrix first since compliance matrix is the inverse of stiffness matrix. The effective constitutive relation can be expressed as

$$\begin{Bmatrix} \overline{\sigma}_{xx} \\ \overline{\sigma}_{yy} \\ \overline{\sigma}_{zz} \\ \overline{\sigma}_{xy} \\ \overline{\sigma}_{yz} \\ \overline{\sigma}_{xz} \end{Bmatrix}_{\text{eff}} = [\bar{C}]_{\text{eff}} \begin{Bmatrix} \overline{\varepsilon}_{xx} \\ \overline{\varepsilon}_{yy} \\ \overline{\varepsilon}_{zz} \\ \overline{\varepsilon}_{xy} \\ \overline{\varepsilon}_{yz} \\ \overline{\varepsilon}_{xz} \end{Bmatrix}_{\text{eff}} \tag{9}$$

Using simple algebraic manipulation, the effective stiffness components can be obtained using FEA program and averaging scheme. For example, when $\overline{\varepsilon}_{xx} = 1$ is applied while all other strain components are zero, the averaged stresses become the first column of the effective stiffness matrix. The value of strain applied to UVE will affect the extent of fiber debonding and will subsequently affect compliance matrix. For different specimen, the value of strain applied to UVE to derive the compliance matrix should be close to the maximum strain. Table 5-3 shows a summary of experimental results and predicted maximum strains. Different strain values are applied to UVE to derive compliance matrix. 0.5% strain value is used for calibration. For $[\pm 60°]_s$ specimen, predicted maximum strain value when applying 2.0% strain to UVE is used for validation. For $[\pm 30°]_s$ and $[\pm 45°]_s$ specimens, 5.0% strain is adopted. The plot of the validation is shown in figure 5-3.

As shown in figure 5-3, besides the $[\pm 75^{\circ}]_s$ specimen data is used for calibration of property of matrix, the other three predicted values show acceptable agreement with experimental results. As mentioned earlier, the deformation of glue is not considered in determining the strain of specimen and this is one cause of the discrepancy between predicted maximum strain values and experimental results of low angle specimens. And due to this cause, the exact strain value at which maximum stress is achieved cannot

be known which also contributes to the discrepancy. Another important cause is the inaccurate estimation of interfacial property. Interfacial property is crucial to the performance of composite materials. However, currently it is difficult to measure the property directly. Here, interfacial property is simply derived from the matrix property.

Table 5-3. Summary of experimental results and model prediction.

Specimen Type	σ_{max} (MPa)	ε_{max}	0.5%	1.0%	2.0%	3.0%	4.0%	5.0%
$[\pm 30^{\circ}]_s$	482	5.80%	---	2.89%	4.01%	4.64%	5.03%	5.33%
$[\pm 45^{\circ}]_s$	207	5.30%	---	1.89%	2.90%	3.48%	3.87%	4.14%
$[\pm 60^{\circ}]_s$	131	2.60%	---	1.59%	2.60%	3.20%	3.61%	3.89%
$[\pm 75^{\circ}]_s$	79	0.60%	0.63%	1.14%	1.92%	2.40%	2.72%	2.94%

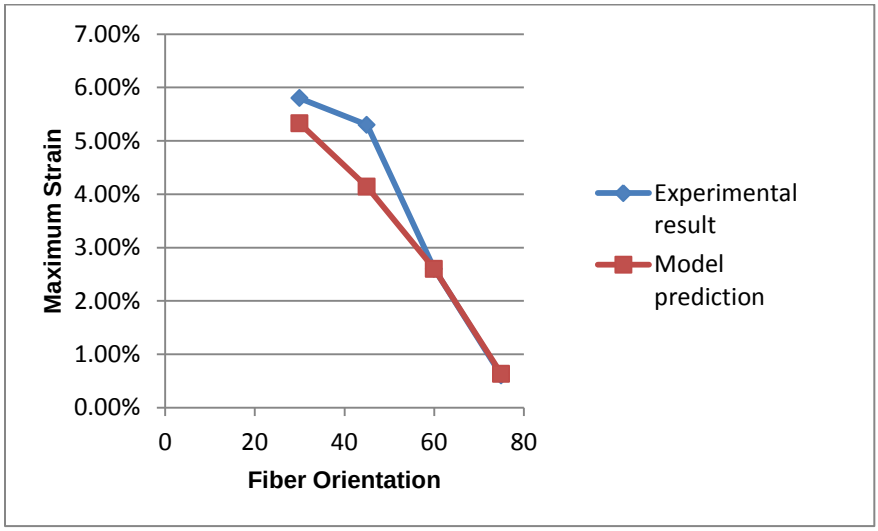

Figure 5-3. Comparison of experimental result and model prediction for validation.

CHAPTER 6
SUMMARY AND DISCUSSION

A surrogate modeling technique is proposed to integrate micro-scale phenomena with macro-scale phenomena to overcome the computational burden in typical multiscale modeling techniques, which often requires massive parallel processing. Kriging surrogate is used due to its ability to estimate uncertainty at unsampled points. Latin hypercube sampling is used to generate random samples of strain values in a reasonable range. Effective stress values are obtained by numerical approach in Abaqus FE program. Surrogate is constructed using Design and Analysis of Computer Experiments (DACE), a Matlab kriging toolbox. In further study, in structural scale modeling, when surrogate is called at every integration point to predict local response, total strain should be provided instead of incremental strain.

In micro scale, UVE approach is used to predict the material point response with given strain values. In this research, we focus on a specific application, i.e. high strain rate impact phenomenon. Due to an extremely short time period of impact, there is no need to consider cyclic loading and unloading scenarios. Instead of conducting a dynamic analysis, quasi-static analysis is used to simulate the micro-scale phenomena by taking the most important factors into consideration. First of all, effect of strain rate on material properties needs to be considered. High strain rates tend to favor the elastic properties of materials. Elasticity is associated with load-bearing performance as embodied in properties such as strength and stiffness. Linear elastic material model is used for both fiber and matrix with the parameters derived from high strain rate tests. Second, fiber cleavage initiates in the micro scale and is one of the major failure mechanisms. It is modeled using level set method. Third, another major mechanism that

contribute to the degradation of local material point is fiber debonding and pullout. It is modeled using cohesive element, which is governed by traction-separation law. Due to the difficulty of obtaining interfacial property through experiments, the property of matrix is assumed to be the upper bound and parameters of traction-separation law are derived from matrix property. Besides, another important failure mechanism is delamination. However, delamination initiates between plies and thus will not be modeled in the unit cell.

High strain rate tests from literature are used to validate the micro-scale model. The split Hopkinson bar was used to conduct the tests. Strain values at which maximum stresses are achieved both from experiments and predicted by UVE model are compared for validation.

LIST OF REFERENCES

1. Kanouté P, Boso DP, Chaboche JL, and Schrefler BA (2009) Multiscale methods for composites: a review. Arch. Comput. Methods Eng.16: 31–75.

2. E W, Engquist B, Li XT, Ren WQ, and Vanden-Eijnden E (2007) Heterogeneous multiscale methods: a review. Commun. Comput. Phys. 2: 367–450.

3. Smit RJM (1998) Toughness of heterogeneous polymeric systems. A modeling approach. PhD thesis, Eindhoven University of Technology, Eindhoven, Netherlands.

4. Feyel F (1999) Multiscale FE2 elastoviscoplastic analysis of composite structures. Comput. Mater. Sci. 16: 344–354.

5. Miehe C, Schröder J, and Schotte J (1999) Computational homogenization analysis in finite plasticity. Simulation of texture development in polycrystalline materials. Comput. Methods Appl. Mech. Eng. 171: 387–418.

6. Terada K, Kikuchi N (2001) A class of general algorithms for multi-scale analysis of heterogeneous media. Comput. Methods Appl. Mech. Eng. 190: 5427–5464.

7. Renard J, Marmonier MF (1987) Etude de l'initiation de l'endommagement dans la matrice d'un matériau composite par une méthode d'homogénisation. Aerosp. Sci. Technol. 6: 37–51.

8. Talreja R, Singh CV (2008) Multiscale modeling for damage analysis. In Kwon, Y. W., Allen, D. H., and Talreja, R., Multiscale modeling and simulation of composite materials and structures. Springer, New York, pp. 529-578.

9. Eshelby JD (1957) The determination of the field of an ellipsoidal inclusion and related problems. Proc. R. Soc. Lond. A 241: 376-396.

10. Hashin Z (1962) The elastic moduli of heterogeneous materials. J. Appl. Mech. 29: 143-150.

11. Mori T, Tanaka K (1973) Average stress in the matrix and average elastic energy of materials with misfitting inclusions. Acta Metall. 21: 571-574.

12. Kim J (2011) Homogenization and uncertainty analysis for fiber reinforced composites. PhD thesis, University of Florida, Gainesville, F.L.

13. Hsueh CH (1992) Interfacial debonding and fiber pullout stresses of fiber-reinforced composites. Mater. Sci. Eng. A 154: 125–132.

14. Zhou LM, Kim JK, and Mai YW (1992) Interfacial debonding and fiber pull-out stresses. J. Mater. Sci. 27: 3155–3166.

15. Henstenburg RB, and Phoenix SL (1989) Interfacial shear strength studies using single filament composite test. Polym. Compos. 10: 389–408.

16. Lin G, Geubelle PH, and Sottos NR (2001) Simulation of fiber debonding with friction in a model composite pushout test. International Journal of Solids and Structures 38: 8547-8562.

17. Chi ZF, Zhou TW, and Shen G (1984) Determination of single fiber strength distribution from fiber bundle testing. J. Mater. Sci. 19: 3319–3324.

18. XIA YM, YUAN JM, and YANG BC (1994) A statistical model and experimental study of the strain-rate dependence of the strength of fibers. Compos. Sci. Technol. 52: 499–504.

19. Zhou YX, Jiang DZ, and Xia YM (2001) Tensile mechanical behavior of T300 and M40J fiber bundles at different strain rate. J. Mater. Sci. 36: 919-922.

20. Goldberg RK, Roberts GD, and Gilat A (2005) Implementation of an associative flow rule including hydrostatic stress effects into the high strain rate deformation analysis of polymer matrix composites. J. Aerosp. Eng. 18: 18-27.

21. Sacks J, Welch WJ, Mitchell TJ, and Wynn HP (1989) Design and analysis of computer experiments. Statistical Science, Vol. 4, No. 4: 409-435.

22. McKay MD, Conover WJ, and Beckman RJ (1979) A comparison of three methods for selecting values of input variables in the analysis of output from a computer code. Technometrics, Vol. 21, No. 2: 239-245.

23. Lophaven SN, Nielsen HB, and Søndergaard J (2002) DACE A Matlab Kriging Toolbox.

24. Kolsky H (1949). An investigation of the mechanical properties of materials at very high rates of loading. Proc. Phys. Soc. 62-B: 676-700.

25. Staab GH, and Gilat A (1995) High strain rate response of angle-ply glass/epoxy laminates. J. Compos. Mater., Vol. 29, No. 10: 1308-1320.

26. Wang Z, and Xia YM (1997). Experimental evaluation of the strength distribution of fibers under high strain rates by bimodal Weibull distribution. Compos. Sci. Technol. 57: 1599-1607.

BIOGRAPHICAL SKETCH

Shu Shang was born in Taikang, China in 1990. He received a Bachelor of Science in mechanical engineering from the Huazhong University of Science and Technology in China in July 2011. For further study, he went to the University of Florida to pursue a master's degree in mechanical engineering and graduated in May 2013.